Catalysis Today 175 (2011) 386–392

Contents lists available at ScienceDirect

Catalysis Today

journal homepage: www.elsevier.com/locate/cattod

Continuous hydrothermal flow syntheses of transition metal oxide doped Ce_xTiO_2 nanopowders for catalytic oxidation of toluene

Xiaole Weng, Jingyi Zhang, Zhongbiao Wu, Yue Liu*

Department of Environmental Engineering, Zhejiang University, Zhejiang Provincial Engineering Research Center of Industrial Boiler & Furnace Flue Gas Pollution Control, Hangzhou 310027, PR China

ARTICLE INFO

Article history:
Received 30 October 2010
Received in revised form 14 February 2011
Accepted 7 April 2011
Available online 19 May 2011

Keywords:
Toluene oxidation
Supercritical water
Transition meal oxide
Ceria
Titania
Continuous

ABSTRACT

A series of transition metal oxides doped Ce_xTiO_2 samples were synthesized using a continuous hydrothermal flow synthesis (CHFS) method. The resultant samples were then investigated using a range of analytical methods, including XPS, X-ray powder diffraction, H_2-TPR, TEM and BET surface area measurements. Experimental results showed that the samples were highly crystalline with remarkably high surface areas (in the range of 200–300 $m^2\ g^{-1}$), which were ca. two-fold higher than those synthesized via more conventional routes. The $Ce_{0.05}TiO_2$ sample revealed a good catalytic performance in toluene oxidation, which was subsequently utilized for the optimization of transition metal oxide doping. After screening MnO_x, CrO_x and CuO_x doping, it was found that they had all led to significant enhancements in the activity for toluene conversion, particularly for CuO_x doped sample, which showed a superior performance (T_{90} = 200 °C) for toluene oxidation, comparable to some noble metal catalysts.

1. Introduction

Pollutants collectively known as "volatile organic compounds" (VOCs) have caused tremendous risks to human health. This leads to an increasing stringency in air pollution control policies in many countries and to some extent facilitates the development of techniques/materials for VOC abatement. Catalytic oxidation of VOCs to less harmful CO_2 and H_2O has been considered as a very effective method for VOC removal. This method is relatively simple and can be operated under moderate temperatures with the assistance of catalysts, whose activities therefore play a crucial role for the oxidation. As such, an explosion in efforts directed towards the syntheses and characterizations of nanocatalysts in the application of VOC oxidation has recently received tremendous attentions.

Towards the development of better catalysts, a number of materials have been studied. However, the vast majority of them are based on noble metals, e.g. Pt, Pd, Au, etc., which are rather expensive and hardly applicable for industry [1–5]. Therefore, researchers have shown strong incentive to search for relatively less expensive catalysts for VOC oxidation. In the last several years, transition metal oxides have been the focus of many researches because of its low price and the ability for catalytic activity enhancement. Wang et al. have reported a CuO catalyst supported by CeO_2, which exhibited a superior activity for catalytic oxidation of toluene [6]. Bertinchamps et al. have screened various TiO_2 supported transition metal oxides (e.g. BiO_x, TaO_x, WO_x, CrO_x, VO_x, MnO_x, etc.) and found that CrO_x, VO_x (however harmful to environment) and MnO_x were the most active oxides for benzene oxidation [7]. However, all these catalysts did not yield comparable activities to noble metals. Furthermore, recent report has demonstrated that ceria could possess large redox property and good dispersion enhancement ability [8], the doping of which with transition metal oxides (e.g. MnO_x supported on TiO_2) exhibited an ultralow light-off temperature T_{20} (temperature of 20% conversion) at ca. 55 °C for selective catalytic reduction (SCR) of NO_x, which is comparable to some noble metal catalysts [9]. Therefore, it may be feasible to investigate the transition metal oxide doped Ce_xTiO_2 catalysts for the application in VOC oxidation, the study of which is however really rare in the literature [10,11].

Preparative approaches also link to the catalytic performance of catalysts to a great extent, attributing to their determinations on component dispersion and resultant surface area. If we limit investigation on materials without considering the preparative methods, the studies are really not comprehensive. There are numerous synthetic routes reported in the literature, e.g. sol–gel route [12], solvothermal route [13], reactive magnetron sputtering route [14], etc., which indeed result in wide ranging outcomes in terms of

Abbreviations: CHFS, continuous hydrothermal flow synthesis; CeMTi, $Ce_{0.035}M_{0.015}TiO_2$ (M = Cu, Mn, Cr) synthesized using a continuous hydrothermal flow synthesis route.

* Corresponding author. Tel.: +86 571 87953088; fax: +86 571 87953088.
E-mail address: bird76@gmail.com (Y. Liu).

0920-5861/$ – see front matter © 2011 Elsevier B.V. All rights reserved.
doi:10.1016/j.cattod.2011.04.016

phase purity and crystallinity. However, most of them cannot afford green synthesis, homogenous doping and scalable for industry. In particular, the vast majority of them involve multiple and time consuming processing steps, which can lead to batch to batch inconsistencies and variations in performance (e.g. the sol–gel route made CeMnTi sample as reported in Ref. [10]).

Following pioneering research of the Arai Group in Japan in the early nineties to develop continuous hydrothermal flow synthesis (CHFS) reactors [15,16], the CHFS methods have been extensively exploited for the syntheses of nanomaterials. The basic CHFS method involves mixing a flow of supercritical water (sc-H_2O, critical temperature T_c = 374 °C; critical pressure, P_c = 22.1 MPa) with a cold flowing aqueous metal salt solution under high pressure to give rapid precipitations (in the mixing zone) and instantaneous growths of well-defined nanoparticles in flow. Thereafter, nanoparticles are continuously collected at atmospheric pressure as slurry from the outlet of the apparatus. The CHFS method has offered a fast route for producing nanomaterials and demonstrated the considerable advantages in terms of green synthesis (only water used as reaction medium) and high reproducibility (due to the simple and controllable process).

The objective of this work is to use the CHFS method for the syntheses of transition metal oxide doped Ce_xTiO_2 nanocatalyst directed towards the application of toluene oxidation. We expect to obtain a relatively less expensive catalyst, which possessed a comparable activity to some noble metal catalysts. To achieve this goal, we first screened diverse Ce_xTiO_2 supports in order to get a suitable composition of M:Ti (M = active specie), followed by hit selections, which were optimized by a sequence of transition metal oxide doping. Based on the literatures, MnO_x, CuO_x and CrO_x were selected for the study in this paper.

2. Experimental details

2.1. Materials

[$Ce(NO_3)_3{\cdot}6H_2O$, ≥99.0%], [$Cu(NO_3)_2{\cdot}3H_2O$, AR], [$Cr(NO_3)_3{\cdot}9H_2O$, AR] and [$Mn(NO_3)_2$, 50 wt% in water] were supplied by Sinopharm Chemical Reagent Co., Ltd. (Shanghai, China). Titanium (IV) bis (ammonium lactate) dihydroxide $[CH_3CH(O-)CO_2NH_4]_2Ti(OH)_2$ (50 wt% in water) was supplied by Alfa Aesar company (UK). All chemicals were used as obtained. Distilled water was used in all experiments.

2.2. Sample characterizations

Freeze-drying was performed using a Vacuum Freeze Dryer, Model LGJ-10C, supplied by Beijing Boyikang Laboratory Instruments Co., Ltd.; the solids were frozen for 4 h and then freeze-dried for 24 h at ≤10 Pa. XRD patterns were obtained by a Rigaku D/Max RA diffractometer with Cu Kα radiation (λ = 0.15418 nm) at 40 kV and 150 mA and at an angle of 2θ from 20° to 80°. BET surface areas (S_{BET}) were determined using N_2 physisorption at 77 K, with a Micromeritics ASSP 2020 equipment. Samples were degassed at 200 °C for 2 h, followed by 5 point BET measurements to yield an average S_{BET} value. Surface elemental analysis was carried out by XPS using a Thermo ESCALAB 250 instrument with Al Kα radiation (photon energy 1486.6 eV) at 150 W. The signal of adventitious carbon (a binding energy of 284.8 eV) had been used to calibrate the binding energy scale for XPS measurements. Curve fits were performed using a Shirley background and a Gaussian peak shape with 30% Lorentzian character. Particle size and morphology of the samples were investigated using a model JEM-2010 high-resolution transmission electron microscope (HR-TEM, 400 kV accelerating voltage) instrument. The molar elemental composition of the products was measured using an Oxford Instruments Inca 400 EDX detector connected to the HR-TEM.

2.3. H_2-TPR measurements

The details of H_2-TPR test and equipment were as follows. The instrument was a TP-5085 supplied by Tianjin Xianquan Industry and Trade Development Co., Ltd., P.R. China. Samples were 0.05 g of mixed oxide powder placed in a fix-bed reactor. The TPR test method used the following steps: (1) pre-treatment step in which samples were heated to 400 °C with a dwell of 1 h and then cooled to 100 °C. The process was operated with a purge of flowing N_2 gas at the rate of 30 mL min^{-1}. The ramp rate was controlled at 10 °C min^{-1}. (2) TPR step in which samples were heated up from 100 °C to 550 °C at 5 °C min^{-1} under flowing H_2/Ar (5% H_2 in Argon) at 30 mL min^{-1} and then cooled to room temperature. The change in thermal conductivity of gas before and after sample was recorded throughout this step. The peak of thermal conductivity detector (TCD) signal was reported as the temperature reduction peak and integrated against time (equate to temperature).

2.4. Catalytic activity test

The activities of the catalysts were measured in a fixed bed reactor. The 6-mm i.d. quartz reactor tube, loaded with 0.5 g catalyst powder, was located in an electrically heated furnace. The flow rate was set to maintain the gas hourly space velocity (GHSV) at 15,000 h^{-1} for all the runs. A nitrogen stream bubbling (flow rate = 9 mL min^{-1}) through a saturator filled with liquid toluene in an ice-water bath, and it was then mixed with 6% O_2/N_2 gas stream, to keep the inlet concentration of gaseous toluene at about 1600 mg m^{-3}. The reactants and products were analyzed using a Fuli 9790 gas chromatograph (GC) equipped with a flame ionization detector (FID). No other carbon-containing organic compounds were detected. The standard deviation of toluene concentration measurement was estimated at ca. ±2%.

2.5. General syntheses

The co-crystallite precursors were manufactured using a three pump CHFS system (Fig. 1). Briefly, pump P1 was used to pump water to the pre-heater (maintained at 450 °C), whilst pump P2 was used to pump the solution with a mixture of salts. Pump P3 was always used for pumping the base solution for the adjustment of pH in the system (but herein used for pumping water only). In all cases, pump speeds were 10 mL min^{-1}, except for the superheated water (20 mL min^{-1}). For the syntheses of Ce_xTiO_2 samples, a solution of cerium nitrate hexahydrate and titanium (IV) bis (ammonium lactate) dihydroxide (with corresponding ratios) in DI water were mixed together and stirred for 2 min. The solution was then continuously pumped (through P2) into the CHFS system (via a HPLC pump), whereupon it was mixed with a P3 pumped flow of water (at point *T*, a ¼ in. swagelok Tee pieces, Fig. 1). Thereafter, the mixture was brought to meet the superheated water feed at 450 °C and 24.1 MPa (in a countercurrent mixer, R, as described elsewhere [17]), whereupon the hydrothermal reaction took place in a continuous fashion. The resultant nanoparticles was cooled via a pipe-in-pipe cooler (C) and then filtered (F) before they had been collected at the exit of a back pressure regulator (BPR, at ambient pressure) for approximately 50 min in 50 mL falcon tubes. Each filled falcon tube was centrifuged (8000 rpm for 3 min). 40 mL of clear liquid was removed and then replaced with 40 mL of clean DI water with shaking to disperse the solids. Each falcon tube was further centrifuged (8000 rpm for 3 min) and the clear liquid was removed again. Eventually, the resultant wet solids were freeze dried. To produce transition metal oxide doping samples, the cor-

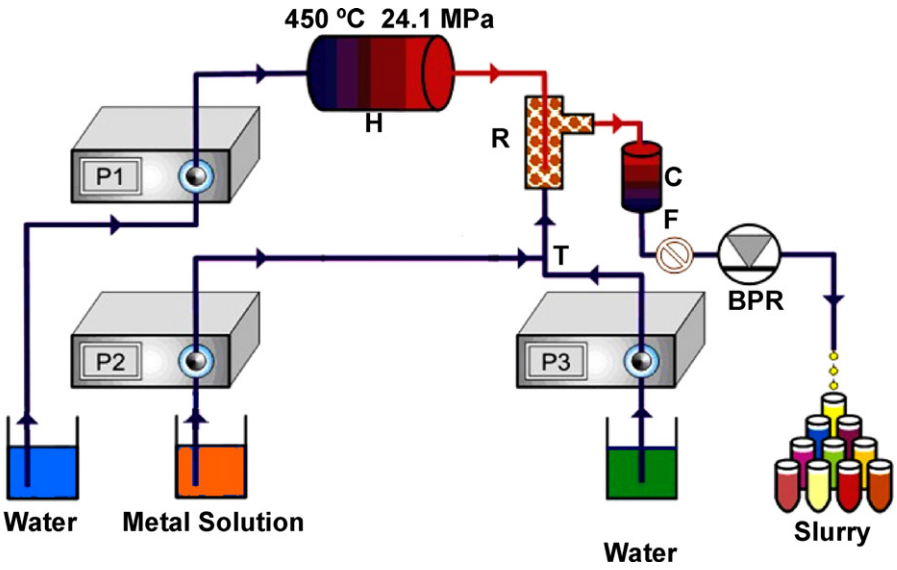

Fig. 1. Schematic representation of the three-pump (P1–P3) continuous hydrothermal flow synthesis system that was used to prepare nanocatalysts. Key: P = pump, C = cooling, F = filter, BPR = back-pressure regulator, R = reactor, H = heater, T = T junction.

responding metal solutions with the ratio of Ce:M:Ti at 0.7:0.3:20 (M = Cr, Cu, Mn) were added into cerium and titanium solution and then pumped via P2 into the system. Thereafter, an identical method to that described earlier was employed.

3. Results and discussion

3.1. Characterizations of Ce_xTiO_2 samples

3.1.1. HR-TEM and BET measurements

Particle morphologies of the as-prepared Ce_xTiO_2 samples were analyzed using a high-resolution TEM. The TEM image showed that well defined polygonal agglomerates with a particle size of 3.8–7.6 nm (5.3 nm in average based on 100 particles measurements, Fig. 2) were obtained for all the samples. The constitutional molar ratios of Ce_xTiO_2 samples were evaluated using a calibrated EDX and gave the Ce:Ti molar ratio relatively close to that expected (e.g. at 0.07:1 of Ce:Ti for $Ce_{0.05}TiO_2$ sample). From the EDX spectrum, it can be deduced that all these observed particles are composed of anatase Ce_xTiO_2 crystallites, as the exposed crystal planes of (1 1 1) were measured with the interplanar spacing of 0.35 nm [18]. The direct synthesis of highly crystalline samples implied a significant advantage of the CHFS route as the vast majority of conventional routes need a further heat-treatment step to yield the highly crystalline products, which hence lead to particle coarsening and reduce the surface area. Indeed, the surface areas measured for the Ce_xTiO_2 samples were in the range of 200–300 $m^2 g^{-1}$, which are about two-fold higher than those synthesized via either wet impregnation (78.7–128.6 $m^2 g^{-1}$) [19] or sol–gel route (57.1–126.1 $m^2 g^{-1}$) [12]. The $Ce_{0.05}TiO_2$ sample had the highest surface area at 269.1 $m^2 g^{-1}$, followed by $Ce_{0.1}TiO_2$ (216.8 $m^2 g^{-1}$), $Ce_{0.2}TiO_2$ (190.4 $m^2 g^{-1}$) and $Ce_{0.25}TiO_2$ (184.3 $m^2 g^{-1}$).

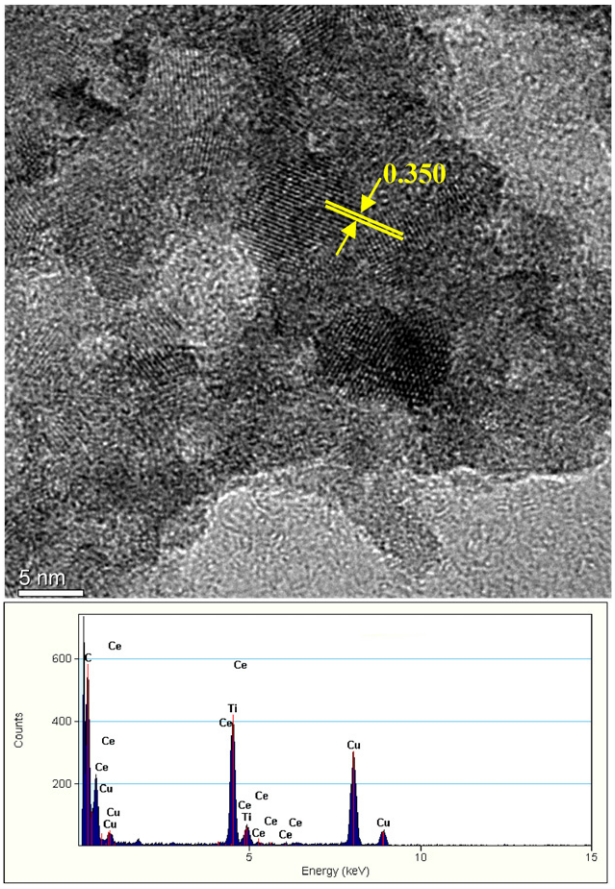

Fig. 2. HR-TEM image of $Ce_{0.05}TiO_2$ sample (bar = 5 nm). The bottom image reveals EDX spectrum of the sample (copper is come from the grids).

3.1.2. X-ray powder diffraction

Phase identity and purity of the Ce_xTiO_2 samples were elucidated using X-ray powder diffraction (XRD), which was directly compared with the Joint Committee on Powder Diffraction Standard (JCPDS) database. The symmetrical peaks of $Ce_{0.05}TiO_2$ and $Ce_{0.1}TiO_2$ samples (Fig. 3) revealed the characteristic peaks of pure anatase TiO_2 (JCPDS 21-1272), which is consistent with the TEM results. NO extra peaks were observed in these two samples, indicating the possible formation of solid solutions. In comparison, the $Ce_{0.2}TiO_2$ and $Ce_{0.25}TiO_2$ samples both revealed the presence of extra CeO_2 characteristic peaks (JCPDS 43-1002), revealing that the CeO_2 did not fully incorporate into the TiO_2 lattice due to the high Ce contents. In addition, a larger 2θ angle shift (comparing to pure TiO_2) was observed in all the samples, indicating a decrease of c

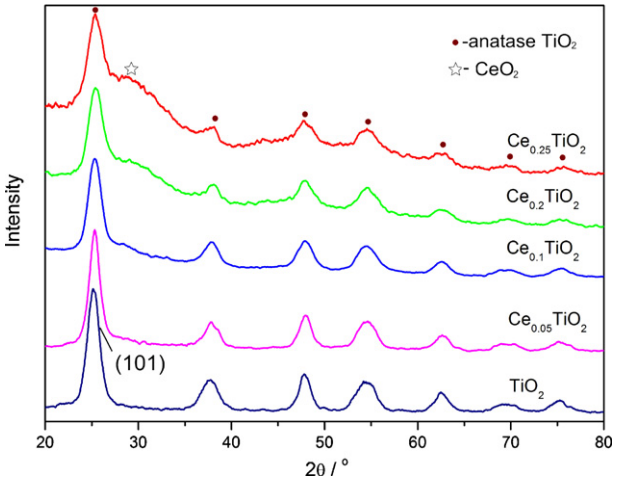

Fig. 3. X-ray powder diffraction patterns of the Ce_xTiO_2 samples.

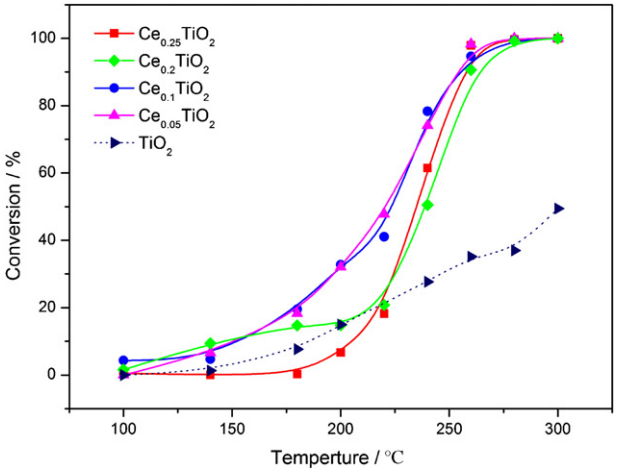

Fig. 4. Temperature dependence of toluene oxidation over the Ce_xTiO_2 samples.

axis parameter in the TiO_2 lattice by the insertion of Ce^{4+} (ionic radius = 0.097 nm) into TiO_2 (ionic radius of Ti^{4+} = 0.053 nm) lattice.

3.1.3. Catalytic performances

Toluene conversion as a function of temperature for the Ce_xTiO_2 samples is given in Fig. 4. The profile revealed that the CeO_2 doping has all increased the catalytic activity compared to pure TiO_2. The $Ce_{0.05}TiO_2$ and $Ce_{0.1}TiO_2$ samples had similar catalytic performance with the total oxidation temperature T_{90} (90% toluene conversion) at ca. 240 °C. With increasing ceria loading, the $Ce_{0.2}TiO_2$ and $Ce_{0.25}TiO_2$ samples yielded very poor activities, where their light-off temperatures, T_{20} (20% toluene conversion), were at ca. 220 °C, much higher than those of $Ce_{0.05}TiO_2$ and $Ce_{0.1}TiO_2$ samples (at 180 °C). This could be caused by the low surface areas of the samples. However, the phase separation of CeO_2 (see XRD results) in these two samples could be also related to their catalytic performances. As suggested from the XPS data, which revealed the surface composition of Ce:Ti at 0.55:1 for $Ce_{0.25}TiO_2$ sample (see Supplementary Fig. S1), the CeO_2 phases appeared to accumulate on the surface of $Ce_{0.25}TiO_2$ sample. The sintering of these CeO_2 phases at evaluated temperatures would greatly shield the exposure of Ce–Ti–O active sites, thereby inhibiting its catalytic activity. Similar phenomena were also observed in the application of selective catalytic reduction of NO with ammonia for Ce_xTiO_2 materials [12,19].

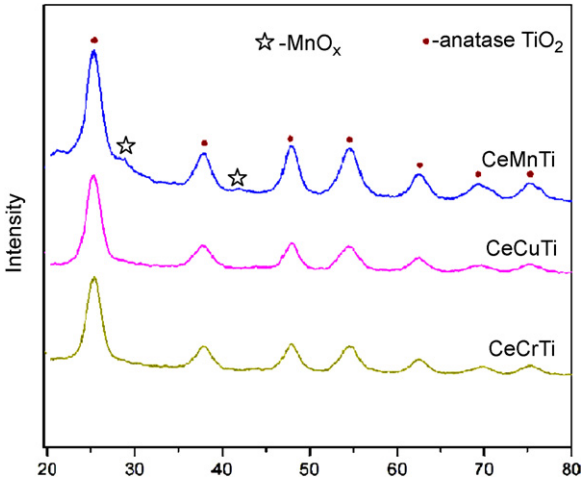

Fig. 5. X-ray powder diffraction patterns of the CeMTi (M = Cr, Cu and Mn) samples.

Since the $Ce_{0.05}TiO_2$ and $Ce_{0.1}TiO_2$ samples performed similar catalytic activities, the lower Ce content of $Ce_{0.05}TiO_2$ sample was then selected for further optimization by transition metal oxide doping (e.g. MnO_x, CrO_x and CuO_x), which were hereafter denoted as CeMnTi, CeCrTi and CeCuTi, respectively.

Note: To compare with more conventional routes, we have also synthesized another $Ce_{0.05}TiO_2$ sample using a wet-impregnation route (in which the ceria was added via simple incipient wetness to a CHFS made TiO_2 support). The catalytic activity of the sample (T_{90} = 280 °C) was observed relatively lower compared with CHFS made sample (T_{90} = 240 °C) (see Supplementary Fig. S2). The low surface area (at 134.5 $m^2\ g^{-1}$) and poor dispersion of ceria (leading to strong sintering at evaluated temperatures) for the wet-impregnation route made sample are strongly proposed for the interpretation.

3.2. Characterizations of CeMTi (M = Mn, Cr and Cu) samples

3.2.1. X-ray powder diffraction and BET surface area measurements

Phase identity and purity of the CeMTi (M = Mn, Cr and Cu) samples were elucidated using X-ray powder diffraction (XRD). The symmetrical peaks of CeMTi samples (Fig. 5) were all consistent with the characteristic peaks of pure anatase TiO_2 (JCPDS 21-1272), except for CeMnTi sample, which showed the presence of very weak MnO_x peaks. The crystallite sizes of the CeMTi samples were calculated using Scherrer equation and the results are listed in Table 1. It was observed that the crystallite sizes of the samples did not follow the sequence of their BET surface areas, where the CeMnTi sample had the lowest surface area but with the smallest crystallite size. This could be caused by the coarsening of MnO_x crystals on the sample surface.

3.2.2. X-ray photoelectron spectroscopy

Table 1 also shows the result of quantitative analysis on the CeMTi samples by XPS. The XPS data revealed that the Ce:Ti ratios were all higher than those expected. For Ce3d spectra, the lack of peak at ca. 917 eV (assigned to Ce^{4+} state [12]) implied that the all CeMTi samples had primary Ce^{3+} state (see Fig. 6a). This is not consistent with the literatures as the vast majority of conventional routes yielded primary Ce^{4+} state for the samples [12,19]. However, this result is promising as it suggested that the ceria phases might be fully doped into the TiO_2 lattices, beneficial to their catalytic activities. The rapid crystallization environment in the CHFS route, which yielded kinetically stable rather than thermodynamically stable products, can be proposed for the interpretation [20].

Table 1
Texture properties, crystallite size and surface compositions of the CeMTi samples.

Samples	S_{BET} ($m^2\ g^{-1}$)	Crystallite size (nm)	XPS				
			Ce	Ti	M	Expected M	O_B/O_{total}
$Ce_{0.05}TiO_2$	269.1	6.6	0.11	1	–	–	0.142
CeMnTi	229.0	4.1	0.14	1	0.038	0.015	0.195
CeCuTi	264.2	4.6	0.11	1	0.018	0.015	0.196
CeCrTi	270.8	4.5	0.12	1	0.014	0.015	0.213

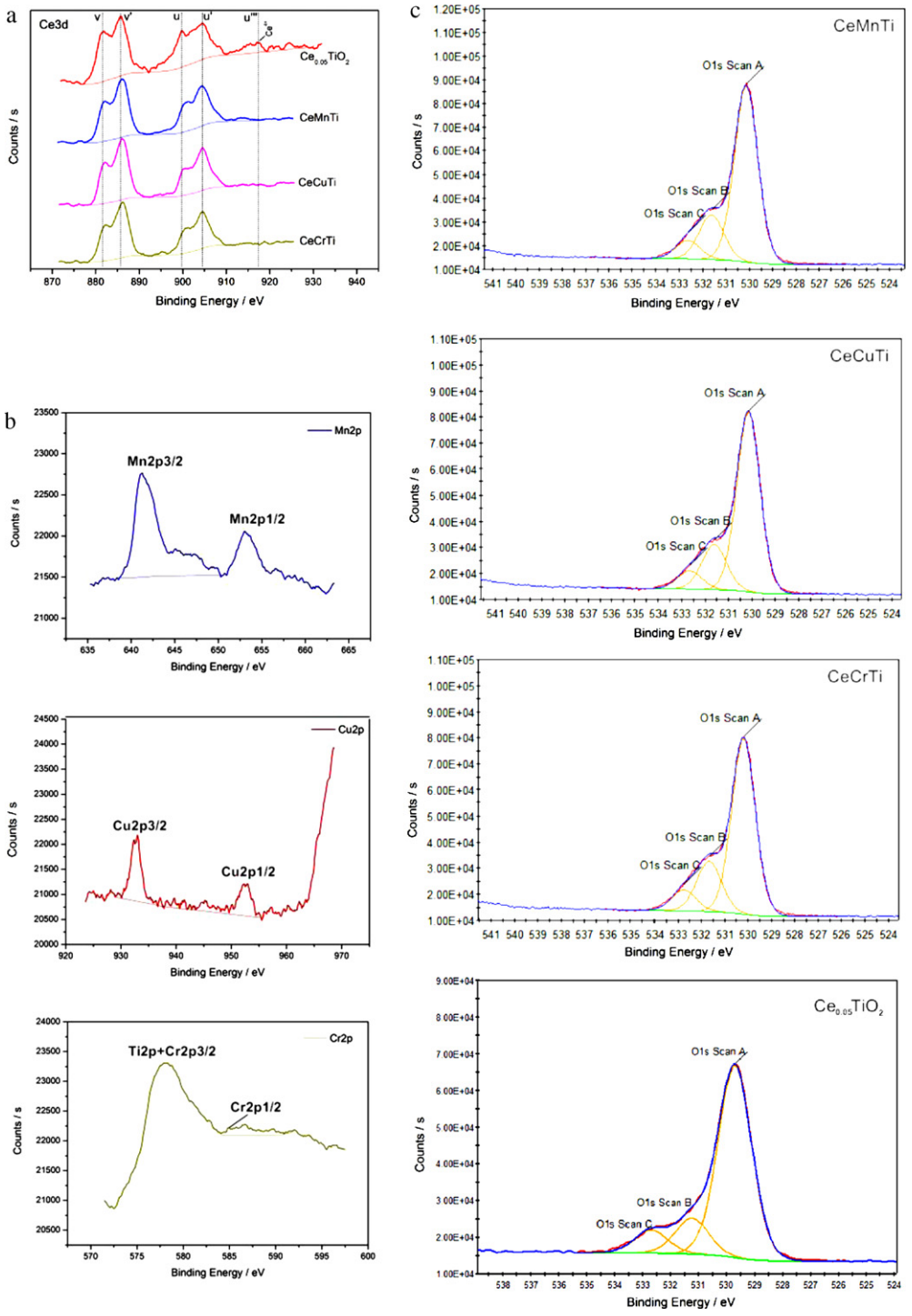

Fig. 6. XPS spectra of (a) Ce3d scan and (b) Mn2p, Cu2p and Cr2p scans and (c) O1s scan for the $Ce_{0.05}TiO_2$ and CeMTi (M = Cr, Cu and Mn) samples.

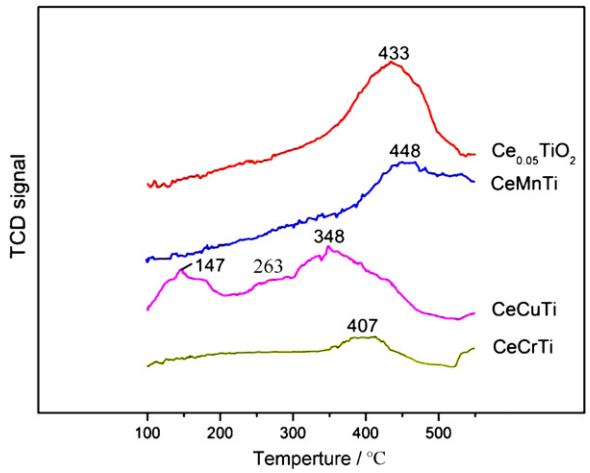

Fig. 7. TPR profiles for the $Ce_{0.05}TiO_2$ and CeMTi (M = Cr, Cu and Mn) samples.

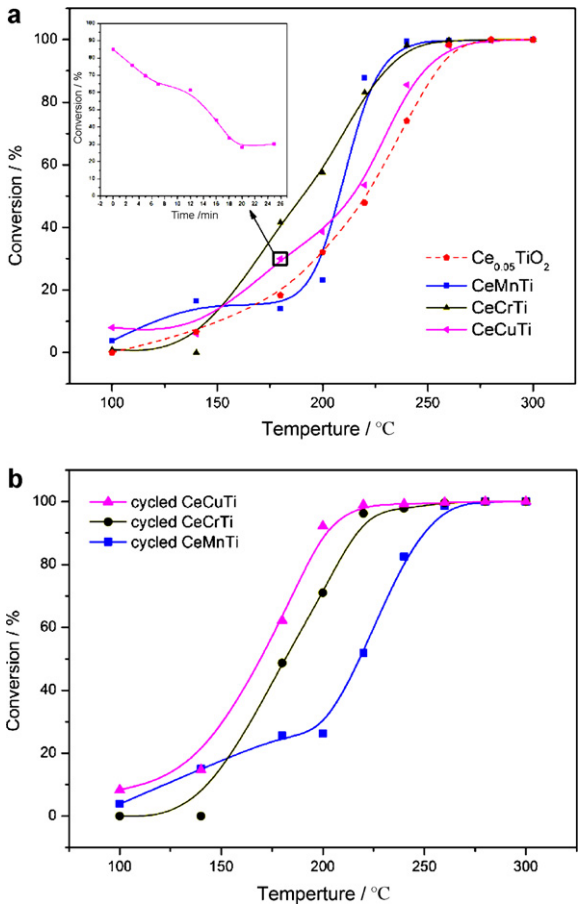

Fig. 8. Temperature dependence of toluene oxidation over (a) $Ce_{0.05}TiO_2$ and CeMTi (M = Cr, Cu and Mn) samples (b) cycled CeMTi samples. The insert in (a) reveals the toluene conversion rate versus testing time for the CeCuTi sample.

The Mn2p spectra in the CeMnTi sample revealed a particularly high amount of MnO_x on sample surface (see Fig. 6b and Table 1). This is consistent with the XRD results and explained the low surface area of the sample because the MnO_x enrichment on sample surface could result in a reduction of its dispersion and hence reduced the surface area. The Mn2p spectrum was observed consisting of a spin–orbit doublet with Mn2p1/2 at ca. 653.3 eV and Mn2p3/2 at ca. 641.7 eV, which revealed the characteristic peaks of a mixed-valence manganese system (Mn^{4+} and Mn^{3+}) [21]. For CeCuTi sample, the Cu2p spectrum also showed a spin–orbit doublet of Cu2p1/2 at ca. 952.4 eV and Cu2p3/2 at ca. 932.7 eV. However, since the Cu2p3/2 value was a little lower than CuO (933.6 eV) and there is no Cu2p3/2 shake-up satellite peak at 940–945 eV, a majority of reduced Cu^+ state in the CeCuTi sample was proposed [11,22]. However, it should be noted that a photo-reduction of Cu^{2+} to Cu^+ might occur during XPS analysis [11]. This implied that the CeCuTi sample might also have Cu^{2+} on its surface. For CeCrTi sample, since the Ti2p loss peak had greatly shielded the Cr2p3/2 peak in the range of 577.0–580.0 eV (corresponding to Cr^{3+} and Cr^{4+} states [23]), the calculation of CrO_x amount was mainly based on the Cr2p1/2 peak, which was present in Table 1.

It is well-known that the chemisorbed oxygen (O_B) is usually relevant to the catalytic activity for VOC oxidation. Therefore, the amounts of surface-absorbed oxygen were also evaluated herein. Fig. 6c revealed the fitted O1s peaks for lattice oxygen O_A (529.0–530.0 eV), chemisorbed oxygen O_B (531.3–531.9 eV) and hydroxyl groups O_C (532.7–533.5 eV) [9]. It can be seen that all the CeMTi samples showed higher O_B than the $Ce_{0.05}TiO_2$ sample (see Table 1), indicating that MO_x doping was beneficial to the catalytic activity. The O_B contents followed the sequence of CeCrTi > CeCuTi ≥ CeMnTi.

3.2.3. H_2-temperature program reduction (H_2-TPR)

H_2-TPR profiles of the CeMTi samples are shown in Fig. 7. The transition metal oxide doping had all promoted the reducibility of the samples except for CeMnTi sample, which yielded the first-reduction peak temperature at ca. 448 °C, higher than that of the $Ce_{0.05}TiO_2$ sample (at 433 °C). Two important aspects, including low surface area and poor MnO_x dispersion, are proposed for the interpretation. The CeCuTi sample revealed three major reduction peaks centered at ca. 147, 263 and 348 °C. The peak at 147 °C could be attributed to the reduction of well-dispersed Cu species; the peak at 263 °C might arise from the reduction of slightly larger Cu species and the peak at 348 °C was mainly originated from the CeO_2 associated with Cu species [8,22]. The CeCrTi sample only revealed one reduction peak centered at ca. 407 °C, attributed to the reduction of CrO_x interacting with CeO_2. From the TPR results, it can be concluded that the reducibility of the CeMTi samples followed the sequence of CeCuTi > CeCrTi > CeMnTi.

3.2.4. Catalytic performances

The light-off curves of toluene oxidation for the CeMTi samples are present in Fig. 8. The activities of CeMTi samples were all higher than those of $Ce_{0.05}TiO_2$ sample, where the CeCrTi and CeCuTi samples revealed better catalytic performances than the CeMnTi sample. This is in accordance with the H_2-TPR, BET and XPS results. However, the activity of CeCuTi sample was rather inhibited at the temperature of ca. 180 °C, where a progressive decrease of the activity with testing time was observed at this temperature (see the insert in Fig. 8a). This could be caused by the presence of CuO_x, which induced a strong sintering of TiO_2 [11,24]. Surprisingly, further cycling these samples (i.e. samples being subjected to repeated tests) had yielded improved activities for CeCrTi and CeCuTi samples. (The CeMnTi sample did not show a significant change after cycled.) Particularly for CeCuTi sample, its light-off temperature T_{20} was decreased from ca. 170 °C to 140 °C and the complete oxidation temperature T_{90} was from 240 °C to 200 °C after cycled. This activity is much higher than those of CuO_x–CeO_2 and CuO_x–TiO_2 materials (prepared via wet-impregnation route) as reported by Wang et al. [6] and reveals a relatively comparable activity to some noble metal catalysts [25,26]. We proposed that the improvement could be due to the increased easily reducible species (e.g. Cu^{2+}

or Cr^{4+}) and enhanced MO_x/CeO_2 interaction in the samples after cycled, which however needs further clarification.

Note: Heat treatment in air in a tube furnace at 300 °C for 1 h of the as-prepared CeCuTi sample also yielded a similar enhanced activity to the cycled CeCuTi sample.

It is worthy to note that although the cycled CeCuTi sample was found possessing a superior catalytic activity, further improvements may be achieved via an optimization in metal oxide composition (i.e. the ratios of Ce:Cu:Ti). However, this will be severely limited by the speed at which large amounts of compositions can be made and tested. Recently, we have developed a modified CHFS reactor, which is able to synthesize a large number of compositionally diverse nanomaterials within a short time [27]. As such, an accelerated discovery of better Ce–Cu–Ti compositions for toluene oxidation can be achieved by using this method, the approach of which is currently pursuing and the result will be reported in due course.

4. Conclusions

We successfully achieved our initial objective using a CHFS route to synthesize relatively less expensive catalysts, which possessed comparable activities to some noble metal catalysts. The CHFS route has yielded products with remarkably high surface area, which is conducive to the catalytic performance in toluene oxidation. It was found that optimization of transition metal oxide doping (e.g. MnO_x, CrO_x and CuO_x) on the $Ce_{0.05}TiO_2$ sample have led to a significant enhancement in the catalytic activity, where the cycled CeCuTi sample (with more Cu^{2+} content) showed a superior performance. We anticipate that the development of this CHFS technique will be of many benefits for better catalyst discovery.

Acknowledgement

The project was financially supported by Changjiang Scholar Incentive Programme (2009), Ministry of Education, P. R. China, China Postdoctoral Science Foundation (20100471738), Zhejiang Higher Education Scientific Research Program (Y200909610).

Appendix A. Supplementary data

Supplementary data associated with this article can be found, in the online version, at doi:10.1016/j.cattod.2011.04.016.

References

[1] J. Bedia, J.M. Rosas, J. Rodriguez-Mirasol, T. Cordero, Appl. Catal. B 94 (2010) 8–18.
[2] K. Bendahou, L. Cherif, S. Siffert, H.L. Tidahy, H. Benaissa, A. Aboukais, Appl. Catal. A 351 (2008) 82–87.
[3] K.J. Kim, H.G. Ahn, Appl. Catal. B 91 (2009) 308–318.
[4] K. Okumura, T. Kobayashi, H. Tanaka, M. Niwa, Appl. Catal. B 44 (2003) 325–331.
[5] H.L. Tidahy, S. Siffert, F. Wyrwalski, J.F. Lamonier, A. Aboukais, Catal. Today 119 (2007) 317–320.
[6] C.H. Wang, S.S. Lin, C.L. Chen, H.S. Weng, Chemosphere 64 (2006) 503–509.
[7] F. Bertinchamps, C. Gregoire, E.M. Gaigneaux, Appl. Catal. B 66 (2006) 1–9.
[8] J.Y. Luo, M. Meng, Y.Q. Zha, L.H. Guo, J. Phys. Chem. C 112 (2008) 8694–8701.
[9] Z.B. Wu, R.B. Jin, Y. Liu, H.Q. Wang, Catal. Commun. 9 (2008) 2217–2220.
[10] D. Yu, Y. Liu, Z. Wu, Catal. Commun. 11 (2010) 788–791.
[11] P.O. Larsson, A. Andersson, J. Catal. 179 (1998) 72–89.
[12] X. Gao, Y. Jiang, Y. Zhong, Z.Y. Luo, K.F. Cen, J. Hazard. Mater. 174 (2010) 734–739.
[13] A.M.T. Silva, B.F. Machado, H.T. Gomes, J.L. Figueiredo, G. Drazic, J.L. Faria, J. Nanopart. Res. 12 (2010) 121–133.
[14] B.S. Liu, X.J. Zhao, N.Z. Zhang, Q.N. Zhao, X. He, J.Y. Feng, Surf. Sci. 595 (2005) 203–211.
[15] T. Adschiri, K. Kanazawa, K. Arai, J. Am. Chem. Soc. 75 (1992) 1019–1022.
[16] T. Adschiri, K. Kanazawa, K. Arai, J. Am. Chem. Soc. 75 (1992) 2615–2618.
[17] E. Lester, P. Blood, J. Denyer, D. Giddings, B. Azzopardi, M. Poliakoff, J. Supercrit. Fluids 37 (2006) 209–214.
[18] B.Q. Jiang, Y. Liu, Z.B. Wu, J. Hazard. Mater. 162 (2009) 1249–1254.
[19] W.Q. Xu, Y.B. Yu, C.B. Zhang, H. He, Catal. Commun. 9 (2008) 1453–1457.
[20] X.L. Weng, B. Perston, X.Z. Wang, I. Abrahams, T. Lin, S.F. Yang, J.R.G. Evans, D.J. Morgan, A.F. Carley, M. Bowker, J.C. Knowles, I. Rehman, J.A. Darr, Appl. Catal. B 90 (2009) 405–415.
[21] S.C. Kim, W.G. Shim, Appl. Catal. B 98 (2010) 180–185.
[22] Z.Q. Zou, M. Meng, L.H. Guo, Y.Q. Zha, J. Hazard. Mater. 163 (2009) 835–842.
[23] R.H. Cheng, C. Xu, Z. Liu, Q. Dong, X.L. He, Y.W. Fang, M. Terano, Y.T. Hu, T.J. Pullukat, B.P. Liu, J. Catal. 273 (2010) 103–115.
[24] C.K. Shin, Y.K. Paek, H.J. Lee, Int. J. Appl. Ceram. Technol. 3 (2006) 463–469.
[25] V.P. Santos, S.A.C. Carabineiro, P.B. Tavares, M.F.R. Pereira, J.J.M. Orfao, J.L. Figueiredo, Appl. Catal. B 99 (2010) 198–205.
[26] Z.M. Liu, R.L. Wang, J.B. Zhong, Y.Q. Chen, S.H. Yan, M.C. Gong, J. Hazard. Mater. 149 (2007) 742–746.
[27] X.L. Weng, J.K. Cockcroft, G. Hyett, M. Vickers, P. Boldrin, C.C. Tang, S.P. Thompson, J.E. Parker, J.C. Knowles, I. Rehman, I. Parkin, J.R.G. Evans, J.A. Darr, J. Comb. Chem. 11 (2009) 829–834.